

The vibrationally mediated photodissociation of Cl₂

E. K. Campbell, A. B. Alekseyev, G. G. Balint-Kurti, M. Brouard, Alex Brown et al.

Citation: *J. Chem. Phys.* **137**, 124310 (2012); doi: 10.1063/1.4754160

View online: <http://dx.doi.org/10.1063/1.4754160>

View Table of Contents: <http://jcp.aip.org/resource/1/JCPSA6/v137/i12>

Published by the [American Institute of Physics](#).

Additional information on *J. Chem. Phys.*


Journal Homepage: <http://jcp.aip.org/>

Journal Information: http://jcp.aip.org/about/about_the_journal

Top downloads: http://jcp.aip.org/features/most_downloaded

Information for Authors: <http://jcp.aip.org/authors>

ADVERTISEMENT



AIPAdvances

Special Topic Section:
PHYSICS OF CANCER

Why cancer? Why physics? [View Articles Now](#)

The vibrationally mediated photodissociation of Cl₂

E. K. Campbell,¹ A. B. Alekseyev,² G. G. Balint-Kurti,³ M. Brouard,^{1,a)} Alex Brown,⁴
R. J. Buenker,² A. J. Johnsen,¹ D. B. Kokh,² S. Lucas,¹ and B. Winter¹

¹The Department of Chemistry, University of Oxford, The Physical and Theoretical Chemistry Laboratory,
South Parks Road, Oxford OX1 3QZ, United Kingdom

²Fachbereich C-Mathematik und Naturwissenschaften, Bergische Universität, Gausstr. 20,
D-42119 Wuppertal, Germany

³Centre for Computational Chemistry, School of Chemistry, University of Bristol,
Bristol BS8 1TS, United Kingdom

⁴Department of Chemistry, University of Alberta, Edmonton, Alberta T6G 2G2, Canada

(Received 24 July 2012; accepted 6 September 2012; published online 27 September 2012)

The photodissociation of vibrationally excited Cl₂($v = 1$) has been investigated experimentally using the velocity mapped ion imaging technique. The experimental measurements presented here are compared with the results of time-dependent wavepacket calculations performed on a set of *ab initio* potential energy curves. The high level calculations allow prediction of all the dynamical information regarding the dissociation, including electronic polarization effects. Using a combination of theory and experiment it was found that there was negligible cooling of the vibrational degree of freedom of the parent molecule in the molecular beam. The results presented are compared with those following the photodissociation of Cl₂($v = 0$). Although the same electronic states are found to be important for Cl₂($v = 1$) as for Cl₂($v = 0$), significant differences were found regarding many of the observables. The overall level of agreement between theory and experiment was found to be reasonable and confirms previous assignments of the photodissociation mechanism. © 2012 American Institute of Physics. [<http://dx.doi.org/10.1063/1.4754160>]

I. INTRODUCTION

The vibrational excitation of molecules in their electronic ground states can modify the pathway of a photodissociation process relative to those in their vibrational ground state. The Franck-Condon factors, the overlap of ground and excited state vibrational wavefunctions, will be different for vibrationally excited reagents. As a result, a molecule may be able to access different parts of the excited state potential, and this may influence, for example, the branching into distinct product channels.¹ A particularly noteworthy example of this *mode specificity* is given by Crim and Schinke on the photodissociation of HOD in the \tilde{A} state.² In their experimental and theoretical study, the authors found that the relative production of OH compared to OD fragments was dependent on the initial vibrational state of the parent molecule and the wavelength used for the photodissociation. They reported that excitation of four quanta in the O–H stretching mode ($4\nu_{\text{OH}}$) led to a selective breaking of the O–H versus the O–D bond. At two of the photolysis wavelengths studied, 239.5 nm and 266 nm, the excess production of OD over OH was as high as 15. However, at the shorter wavelength of 218.5 nm the OD and OH products were found to be formed in equal amounts. Wavepacket calculations on an *ab initio* potential surface showed that promotion of the molecule from high, $4\nu_{\text{OH}}$, O–H stretching levels below the barrier separating the OD and OH product channels gave rise to a large Franck-Condon overlap between the OD + H channel continuum wavefunction and the HOD vibrational wavefunction,

ultimately resulting in a large excess of OD products. On the other hand, excitation at the shorter wavelength, 218.5 nm, was shown to access the \tilde{A} state potential above the energetic barrier separating the OD + H and OH + D product channels. In this region, the continuum wavefunctions for both channels were shown to be significant, allowing for comparable Franck-Condon overlap of the initial vibrational wavefunction with the continuum wavefunctions for dissociation into OD + H and OH + D.²

Another interesting example of vibrationally mediated photochemistry has been given by Alekseyev *et al.*³ in their *ab initio* calculations of the HI photodissociation in its first absorption band. It has been shown that a strong and opposite dependence of the parallel $a^3\Pi_0^+ \leftarrow X^1\Sigma^+$ and perpendicular $a^3\Pi_1, A^1\Pi \leftarrow X^1\Sigma^+$ transition moments on the H–I distance allows one to increase the $I^*(^2P_{1/2})/I(^2P_{3/2})$ branching ratio in the HI photodissociation from the maximum value of ~ 0.5 for excitation from $X, v'' = 0$ to values up to 0.8–0.9 for $v'' = 1, 2$. This theoretical prediction has been confirmed later by Camden *et al.*⁴ in their experimental study of the HI($v'' = 2$) photolysis in the 297–350 nm spectral range. As has been demonstrated in Ref. 5, a small numerical correction for an error in the computed $A^1\Pi$ correlation energy leads to an excellent agreement of the experimental and calculated I^*/I branching ratio in the HI photodissociation. Analogous *ab initio* analysis has also been carried out for the vibrationally mediated photodissociation of CH₃I.^{6,7}

The present study is concerned with the photodissociation of vibrationally excited Cl₂($v = 1$) following excitation into the first absorption band. To our knowledge, there has been only one previous determination of the atomic

^{a)}Electronic mail: mark.brouard@chem.ox.ac.uk.

polarization following the photodissociation of $\text{Cl}_2(v=1)$, by Zare and co-workers,⁸ and that was performed at a single wavelength of 470 nm. In a recent paper,⁹ experimental results following the photodissociation of $\text{Cl}_2(v=0)$ at a range of wavelengths were compared to the results of time-dependent wavepacket calculations¹⁰ performed on a set of high level *ab initio* potential energy curves.¹¹ The experimental results, which included the first determination of high order ($K=3$) electronic orientation moments of $\text{Cl}(^2\text{P}_{3/2})$ atoms, were, in general, in good agreement with the high level theory. In the present work, the recent time-dependent wavepacket calculations¹⁰ are extended to encompass the photodissociation of vibrationally excited $\text{Cl}_2(v=1)$, in order to compare with experimental measurements.

The recent theoretical work¹⁰ appears to confirm the previously understood mechanism for the photodissociation of this diatomic molecule,^{12–14} with the majority of ground state $\text{Cl}(^2\text{P}_{3/2})$ products believed to arise following photoexcitation to the repulsive $\text{C}^1\Pi_{1u}$ state (see Ref. 10 for the term symbol notation employed here). In addition to the products formed following adiabatic dissociation on the $\text{C}^1\Pi_{1u}$ state, an additional contribution to the $\text{Cl}(^2\text{P}_{3/2}) + \text{Cl}(^2\text{P}_{3/2})$ product channel (labelled $\text{Cl} + \text{Cl}$) arises following a non-adiabatic transition to the $\text{A}^3\Pi_{1u}$ state at large distances, where the two potential energy curves are close in energy. Becoming increasingly important at longer wavelengths is the $\text{Cl}(^2\text{P}_{3/2}) + \text{Cl}(^2\text{P}_{1/2})$ product channel (labelled $\text{Cl} + \text{Cl}^*$), which arises following spin-forbidden excitation to and adiabatic dissociation on the $\text{B}^3\Pi_{0+u}$ state. At shorter wavelengths, non-adiabatic transitions from the photoexcited $\text{C}^1\Pi_{1u}$ state give rise to population in both the $(1)^3\Sigma_{1u}^+$ and $(1)^3\Delta_{1u}$ states which correlate with the $\text{Cl}(^2\text{P}_{3/2}) + \text{Cl}(^2\text{P}_{1/2})$ asymptote.

The paper is organized as follows. In Sec. II, the details of the theoretical time-dependent wavepacket calculations are set out. Experimental and data analysis details are very briefly described in Sec. III. The results from this theoretical calculation are presented in Sec. IV, where they are compared with the experimental measurements made here, and with the recent theoretical study on the photodissociation of $\text{Cl}_2(v=0)$.¹⁰ The paper concludes with a short summary and suggestions for topics of future study.

II. THEORETICAL DETAILS

The theoretical procedure used here to investigate the photodissociation of vibrationally excited Cl_2 is identical to the method set out by Balint-Kurti and co-workers for the photodissociation of the hydrogen halides^{15–19} and the recent study on the photodissociation of $\text{Cl}_2(v=0)$,¹⁰ and only the principles and key equations are described here. The fully quantum mechanical method seeks to solve the time-dependent Schrödinger equation,

$$i\hbar \frac{\partial}{\partial t} \Theta(R, t) = \hat{H}(R) \Theta(R, t), \quad (1)$$

where the time-independent Hamiltonian $\hat{H}(R)$ includes the radial nuclear kinetic energy operator, the electrostatic poten-

tial, $V(R)$, and the spin-orbit operator, $\hat{H}_{\text{SO}}(R)$,^{18,19}

$$\hat{H} = -\frac{\hbar^2}{2\mu} \frac{d^2}{dR^2} + \frac{\hbar^2}{2\mu R^2} \hat{L}^2 + V(R) + \hat{H}_{\text{SO}}(R). \quad (2)$$

Molecular rotational motion is neglected in the current treatment, with the term $\frac{\hbar^2}{2\mu R^2} \hat{L}^2$ set to zero. Note that this is equivalent to neglecting the effect of Coriolis coupling, which couples states that differ in Ω by ± 1 . The total Hamiltonian can therefore be represented by the total potential, $V_{\text{tot}} = V(R) + \hat{H}_{\text{SO}}(R)$, and nuclear kinetic energy terms, $-\frac{\hbar^2}{2\mu} \frac{d^2}{dR^2}$.^{18,19}

An initial wavepacket at time zero, $\Theta(R, t=0)$, is generated on the excited state potential via the product of the ground electronic state nuclear wavefunction, $\Psi_{\Omega_i}(R)$, with the electronic transition dipole moment function, $d_q(R)$,^{18,19}

$$\Theta(R, t=0) = d_{q'}(R) \Psi_{\Omega_i}(R). \quad (3)$$

When more than one state is involved, $\Theta(R, t)$ can be written as^{18,19}

$$\begin{pmatrix} \chi_1(R, t=0) \\ \chi_2(R, t=0) \\ \vdots \\ \chi_n(R, t=0) \end{pmatrix} = \begin{pmatrix} d_q^1(R) \Psi_{\Omega_i}(R) \\ d_q^2(R) \Psi_{\Omega_i}(R) \\ \vdots \\ d_q^n(R) \Psi_{\Omega_i}(R) \end{pmatrix}, \quad (4)$$

where $\chi_n(R, t)$ and $d_q^n(R)$ represent the wavepacket and transition dipole moment associated with the excited state n . The resulting wavepacket(s) are then propagated according to the formal solution of the time-dependent Schrödinger equation

$$\Theta(R, t) = \exp^{-i\hat{H}t/\hbar} \Theta(R, t=0). \quad (5)$$

The ground electronic state nuclear wavefunction is calculated using the Fourier grid Hamiltonian technique.²⁰ In this method, numerical calculation of bound state eigenvalues and eigenfunctions can be made at a series of discrete grid points.²⁰ Following their creation, the wavepackets are propagated using the Chebychev method for the time evolution operator $\exp^{-i\hat{H}t/\hbar}$.²¹ A Fourier transform method²² is used to evaluate the action of the kinetic energy operator on the wavepacket. In order to avoid the so-called aliasing complications which can arise in this method the wavepacket must be prevented from reaching the edge of the grid. This is accomplished using a complex cubic absorbing potential.²³

In order to take into account non-adiabatic effects the calculation is performed using two different electronic bases. In the first electronic basis, which is referred to as the fully adiabatic basis, $V_{\text{tot}}(R) = V(R) + H_{\text{SO}}$ is diagonal and off diagonal matrix elements, which couple different electronic states of the same Ω , arise due to the nuclear kinetic energy term, $-\frac{\hbar^2}{2\mu} \frac{d^2}{dR^2}$. On the other hand, in the diabatic basis the good quantum numbers are Λ and Σ , $-\frac{\hbar^2}{2\mu} \frac{d^2}{dR^2}$ and $V(R)$ are diagonal, with off diagonal terms in the spin-orbit operator, \hat{H}_{SO} .^{24,25} The two bases are related by a unitary transformation.^{18,19,24,25}

Propagation of the excited wavepackets, using the Chebychev method,²¹ is performed in a series of short time steps. As discussed by Balint-Kurti and co-workers,^{18,19} initially a fast Fourier transform is used to convert the diabatic wavepackets from the position to momentum representation. The reason for performing a transformation to the momentum representation is to simplify the computation of the effect of the nuclear kinetic energy operator, which becomes a multiplication as opposed to a derivative.^{18,19,22,26} The wavepackets are then transformed back to the position representation using an inverse fast Fourier transform and converted to the adiabatic representation. The effect of the total potential energy term, V_{tot} , is then calculated. Finally, a new set of diabatic wavepackets is generated, completing the calculation for the time step.^{18,19}

Analysis of the wavepackets can yield the absorption cross section and photofragment T matrix elements over a wide range of excitation energies. The autocorrelation function, $A(t)$, is the overlap of the initial wavepacket with that observed at time t , and can be calculated after each time step^{18,19}

$$A(t) = \sum_n \int_0^\infty \chi_n^*(R, t=0) \chi_n(R, t) dR, \quad (6)$$

where the summation is over all states n . Taking the Fourier transform of the autocorrelation function, $A(t)$, over time yields the absorption cross section, $\sigma^{\text{abs}}(\nu)$,^{18,19,27–29}

$$\sigma^{\text{abs}}(\nu) = \frac{\pi \nu}{3c\epsilon_0 \hbar} \int_{-\infty}^{+\infty} \exp[i(E_{\text{int}} + h\nu)t/\hbar] A(t) dt, \quad (7)$$

where E_{int} is the energy of the initial state.

The partial cross sections and photofragment T matrix elements are computed by analysis of the wavepackets at large values of internuclear distance, $R = R_\infty$. As shown by Balint-Kurti and co-workers, for dissociation into a particular channel, n , the photofragment T matrix element may be expressed as^{15,16}

$$\langle \Psi_{n,\Omega}^-(R, E) | \hat{d}_q | \Psi_{\Omega_i} \rangle = i \left(\frac{\hbar^2 k}{2\pi \mu} \right)^{1/2} \exp(-ikR_\infty) A_n(R_\infty, E), \quad (8)$$

where $A_n(R_\infty, E)$ is given by^{15,16}

$$A_n(R_\infty, E) = \frac{1}{2\pi} \int_0^\infty \chi_n(R_\infty, t) \exp[i(E_{\text{int}} + h\nu)t/\hbar] dt, \quad (9)$$

where k represents the asymptotic wavevector and μ the reduced mass of the photofragments.^{15,16} The value of R_∞ is chosen to be sufficiently large such that the potentials have, within some small error margin, reached their asymptotic values. The analysis, performed by taking cuts through the wavepackets at R_∞ , takes place in the adiabatic representation.

As described in Ref. 10, the calculation was performed on a set of 10 *ab initio* potential energy curves.¹¹ The potentials included in the calculation, in both the diabatic and adiabatic representations, are shown in Fig. 1 and listed in

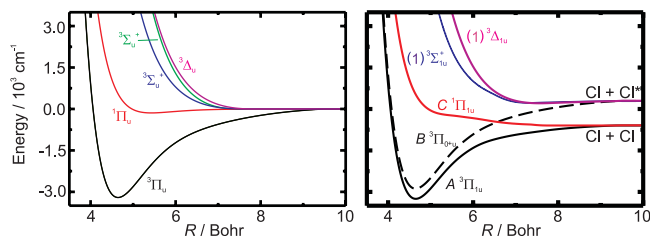


FIG. 1. The relevant diabatic (left) and adiabatic (right) potentials¹¹ for the electronically excited states of Cl_2 included in the dynamics calculation.

Table I. Constant (R independent) values of the *ab initio* transition dipole moments¹¹ in the adiabatic representation were used in the calculation, as listed in Table II. The details of all parameters used to perform the dynamical calculation are provided in Table III.

III. EXPERIMENTAL AND ANALYSIS PROCEDURES

The experiments were carried out using a standard velocity map³⁰ ion imaging³¹ apparatus, which has been described in detail in previous publications (see, for example, Refs. 9 and 32 for more detail). The present experiments on the photodissociation $\text{Cl}_2(v=1)$ were performed concurrently with our most recent work on the photodissociation of $\text{Cl}_2(v=0)$, and the experimental details are identical to those described in Ref. 9. Cl_2 was introduced into the velocity map ion imaging system via a skimmed molecular beam. Previous experiments⁹ suggest a parent molecular rotational temperature of $\lesssim 10$ K. The $^{35}\text{Cl}(^2\text{P}_{3/2})$ photofragments were ionized using the $(2+1)$ REMPI transitions via the $^2\text{P}_{1/2}$ and $^2\text{D}_{5/2}$ intermediate states at 234.5 nm and 236.2 nm, respectively. The probe laser power was attenuated so as to avoid saturation of both the 2 photon step of the $(2+1)$ REMPI transition and the ion counting algorithm. During image acquisition the probe laser was scanned over the Doppler profile of the REMPI transition to obtain equal detection sensitivities for all product velocities.

Images were collected in several pump-probe geometries using both REMPI transitions for the $^{35}\text{Cl}(^2\text{P}_{3/2})$ atomic products. Labels are assigned to the different pump-probe geometries in order to describe the polarization of light in the

TABLE I. The ungerade electronic states of the Cl_2 molecule correlating with two $^2\text{P}_J$ Cl fragments which are included in the dynamics calculations. Hund's case (c) labels are given in parenthesis.

State	Adiabatic correlation
$^3\Pi_u(2_u)$	$\text{Cl}(^2\text{P}_{3/2}) + \text{Cl}(^2\text{P}_{3/2})$
$A^3\Pi_u(1_u)$	$\text{Cl}(^2\text{P}_{3/2}) + \text{Cl}(^2\text{P}_{3/2})$
$C^1\Pi_u(1_u)$	$\text{Cl}(^2\text{P}_{3/2}) + \text{Cl}(^2\text{P}_{3/2})$
$^3\Delta_u(3_u)$	$\text{Cl}(^2\text{P}_{3/2}) + \text{Cl}(^2\text{P}_{3/2})$
$B^3\Pi_u(0_u^+)$	$\text{Cl}(^2\text{P}_{3/2}) + \text{Cl}(^2\text{P}_{1/2})$
$(1)^3\Sigma_u^+(1_u)$	$\text{Cl}(^2\text{P}_{3/2}) + \text{Cl}(^2\text{P}_{1/2})$
$^3\Delta_u(2_u)$	$\text{Cl}(^2\text{P}_{3/2}) + \text{Cl}(^2\text{P}_{1/2})$
$(1)^3\Delta_u(1_u)$	$\text{Cl}(^2\text{P}_{3/2}) + \text{Cl}(^2\text{P}_{1/2})$
$^3\Sigma_u^+(1_u)$	$\text{Cl}(^2\text{P}_{1/2}) + \text{Cl}(^2\text{P}_{1/2})$

TABLE II. *Ab initio* transition dipole moments (TDM)¹¹ used in the wavepacket dynamics calculation.

State	TDM (D)
A $^3\Pi_{1u}$	0.021
B $^3\Pi_{0u}^+$	0.060
C $^1\Pi_{1u}$	0.347
(1) $^3\Sigma_u^+$	0.010

time-of-flight frame (see, for example, Refs. 9 and 32). The first letter (or number) of each label corresponds to the pump and the second to the probe laser polarization. V and H refer to geometries in which the electric vector of the light lies perpendicular or parallel to the image plane, respectively. (Note that the molecular beam direction lies perpendicular to the image plane.) In addition to H and V geometries, images were also collected with the (linearly polarized) electric vector of the pump laser at $\pm 45^\circ$ to the time-of-flight axis, as well as with both left (L) and right (R) circularly polarized photolysis and probe radiation. The use of both a large number of laser polarization geometries and two REMPI transitions allowed for the determination of the $K = 1$ –3 moments of the electronic angular momentum distribution for the $\text{Cl}(^2P_{3/2})$ atomic photofragments.

Extraction of data from the experimental ion images was performed following the Fourier moment analysis procedure,³³ as described in detail by Brouard *et al.* previously.^{9,32} This procedure allows determination of the speed distribution, the speed dependence of the spatial anisotropy parameter, and the speed dependence of the laboratory frame polarization parameters from a set of velocity mapped ion images. Since the analysis procedure has been discussed in detail in several previous publications,^{9,32–36} the reader is referred to this previous work for more information. A Monte Carlo based procedure (see, for example, Ref. 33) was used to determine the errors on the fitted coefficients and angular distribution, which unless otherwise stated are quoted at the 1σ level.

TABLE III. Parameters used in the QM wavepacket calculations.

Parameter	Value
Total number of propagation time steps	32 768
Time step (a.u.)	0.5
No. of grid points	2048
Grid spacing (bohr)	0.0075
Grid range (bohr)	3.2–18.5
Analysis distance (bohr)	15.0
Start of damping potential (bohr)	15.5
Damping parameter (bohr)	0.0594
No. of Chebychev polynomials	14

IV. RESULTS AND DISCUSSION

A. Ion images and fits

Ion images presented here were obtained following the photodissociation of Cl_2 at six wavelengths between 376 nm and 470 nm. At short wavelengths, 376–420 nm, the dissociation of $\text{Cl}_2(v = 1)$ gives rise mainly to the ground state product channel, $\text{Cl}(^2P_{3/2}) + \text{Cl}(^2P_{3/2})$, whereas dissociation at 450 nm and 470 nm gives rise almost exclusively to the excited state product channel, $\text{Cl}(^2P_{3/2}) + \text{Cl}(^2P_{1/2})$. The electronic polarization of the $\text{Cl}(^2P_{3/2})$ photofragments can be observed by inspecting raw ion images recorded with the same pump/photolysis polarization but different probe polarization. As an example, a selection of ion images obtained following photodissociation of Cl_2 at 398 nm is shown in Fig. 2. Here, the three features in the ion images correspond to the dissociation of $\text{Cl}_2(v = 0)$ into the ground and excited state product channels, and to the dissociation of $\text{Cl}_2(v = 1)$ to the ground state product channel. The electronic alignment in the ground state product channel can be seen in differences between the VV and VH ion image geometries, and, more noticeably, in the associated Fourier moments shown in the panels on the right.

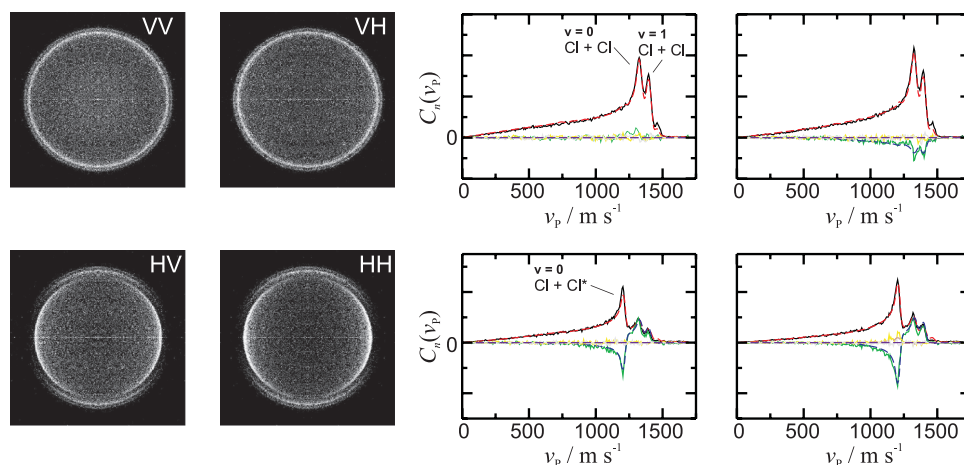


FIG. 2. $\text{Cl}(^2P_{3/2})$ ion images (left panels), and corresponding Fourier moments (—) and fits (---) (right panels) for linearly polarized pump and probe radiation obtained using the $^2P_{1/2} \leftarrow ^2P_{3/2}$ transition following photodissociation at 398 nm. The Fourier moments are colour coded, C_0 (black), C_2 (green), C_4 (yellow), C_6 (grey).^{32,33}

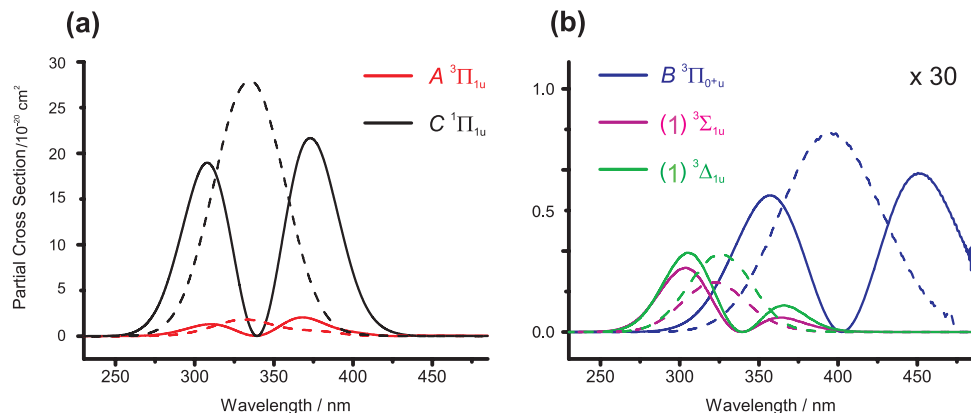


FIG. 3. Calculated partial photodissociation cross sections showing the contributions from all of the states included in the $Cl_2(v=1)$ dynamical calculations (—). The data are compared with similar results for $Cl_2(v=0)$ (---).¹⁰ (a) Partial photodissociation cross sections for states correlating with the ground state product channel (Cl + Cl). (b) Closeup of partial photodissociation cross sections for states correlating with the excited state product channel (Cl + Cl*). The data for $Cl_2(v=1)$ (—) are compared with those for $Cl_2(v=0)$ (---).¹⁰

B. Partial photodissociation cross sections

The partial photodissociation cross sections for all states correlating with the $Cl(^2P_{3/2}) + Cl(^2P_{3/2})$ and $Cl(^2P_{3/2}) + Cl(^2P_{1/2})$ product channels, calculated from the square of the T matrix elements returned from the dynamics calculation, are shown in Fig. 3. Superimposed as dashed lines on the same plots are the partial cross sections following the photodissociation of $Cl_2(v=0)$.¹⁰ The partial cross sections yield information about the probability that the photofragment will be found in a specific adiabatic state following photodissociation. Figures 3(a) and 3(b) show the cross sections relevant for dissociation into the ground (Cl + Cl) and excited state (Cl + Cl*) product channels, respectively.

The same states that are significant for the dissociation of $Cl_2(v=0)$ are found to be important in the dissociation of $Cl_2(v=1)$ molecules. However, the partial photodissociation cross sections themselves, and the wavelengths at which they become important, change significantly compared with those for $Cl_2(v=0)$. Most strikingly, as a consequence of the reflection principle,³⁷ the partial cross sections for all states possess minima at certain wavelengths following dissociation from $Cl_2(v=1)$. The minima appear because the dissociation is a direct process, and the shape of the partial cross sections are primarily determined from the internuclear wavefunction of the ground electronic state. In this direct dissociation process, the shape of the partial cross sections arises from a projection of the $Cl_2(v=1)$ internuclear wavefunction onto the continuum wavefunction of the repulsive excited state potential. As a result, the cross sections for the $Cl_2(v=1)$ calculation possess a minimum near the position of the maximum in the $Cl_2(v=0)$ cross sections.

For dissociation to the ground state product channel (Cl + Cl) only the $C^1\Pi_{1u}$ and $A^3\Pi_{1u}$ states are predicted to be important. The partial cross sections for these two states, Fig. 3(a), both possess a minimum at around 340 nm. Recall that the $A^3\Pi_{1u}$ state is primarily populated through non-adiabatic transition from the $C^1\Pi_{1u}$ state.^{9,10,12–14} Direct excitation to the $A^3\Pi_{1u}$ state plays only a very minor role in the non-adiabatic calculations,^{9,10} and therefore the minimum in the partial absorption cross sections for the $C^1\Pi_{1u}$

and $A^3\Pi_{1u}$ occur at the same wavelength. Furthermore, the $Cl_2(v=1)$ partial cross section for the $C^1\Pi_{1u}$ state is seen to be significant at much longer and shorter wavelengths compared to the dissociation from $Cl_2(v=0)$. This has implications for the branching into the two product channels, as discussed below in Sec. IV D. For the excited state product channel (Cl + Cl*), the $B^3\Pi_{0+u}$, $(1)^3\Sigma_{1u}^+$, and $(1)^3\Delta_{1u}$ states are important, with population in the latter two arising primarily following photoexcitation to the $C^1\Pi_{1u}$ state. Since dissociation on the $(1)^3\Sigma_{1u}^+$ and $(1)^3\Delta_{1u}$ state potentials arises mainly following a non-adiabatic transition from the $C^1\Pi_{1u}$ state (as opposed to direct photoexcitation), the minima in the partial cross sections appear at very close to the same wavelength as that for the $C^1\Pi_{1u}$ state. The $Cl_2(v=1)$ partial cross section for the $B^3\Pi_{0+u}$ state, shown in Fig. 3(b), extends to much longer wavelengths than that for $Cl_2(v=0)$ photodissociation. Interestingly, the partial cross sections for the $(1)^3\Sigma_{1u}^+$ and $(1)^3\Delta_{1u}$ states appear somewhat different in shape to those for all other states. In particular, for these two states larger cross sections are seen on the short wavelength side of the minimum, whereas for all other states the opposite is true, illustrating the increasing importance of the non-adiabatic transition from the $C^1\Pi_{1u}$ to $(1)^3\Sigma_{1u}^+$ state at shorter wavelengths.

In the previous work of Kokh *et al.*,¹¹ reporting the potential energy curves of Cl_2 employed in the present study, the authors also perform adiabatic calculations of the partial and total absorption cross sections into the first absorption band from $Cl_2(v=0)$ and $(v=1)$. The calculations presented therein¹¹ differ from those shown here in a number of respects. First, in the present work the potentials have been fit, as described previously,¹⁰ to potential energy functions, whereas in the work of Kokh *et al.* the potential energy points were smoothed using a cubic spline. This leads to small percentage differences in the absorption cross sections calculated in the case of adiabatic dynamics, and in the Cl*/Cl branching fractions discussed in Sec. IV D. Second, the present calculations are of partial photodissociation cross sections, as opposed to partial absorption cross sections, and also include non-adiabatic (radial derivative coupling) effects. This means

that direct comparison of the present results with the adiabatic partial absorption cross section calculations of Kokh *et al.*¹¹ is not possible. In particular, non-adiabatic behaviour has a significant effect on the partial photodissociation cross sections for some of the states involved.¹⁰ As noted above, the most noticeable example of this is the partial photodissociation cross section via the $A^3\Pi_{1u}$ state, which is significantly shifted in wavelength through non-adiabatic coupling to the $C^1\Pi_{1u}$ state, compared to the adiabatic calculation of the partial absorption cross section to the $A^3\Pi_{1u}$ state.

C. Vibrational “temperature” of the molecular beam

Surprisingly, large signal levels identified as arising from the photodissociation of $\text{Cl}_2(v=1)$ have been observed experimentally. Attempts have therefore been made to assign the likely vibrational temperature associated with the molecular beam using a combination of both experiment and theory. The partial cross sections, or rather, the sum of the partial cross sections relevant to the dissociation into the ground and excited state product channels have been determined from both the $\text{Cl}_2(v=0)$ ¹⁰ and $\text{Cl}_2(v=1)$ calculations. Use of the ratio of these two quantities, $\sigma_{v=1}/\sigma_{v=0}$, weighted by the parent molecule vibrational populations, therefore allows simulation of relative signals arising from Cl_2 in $(v=0)$ and $(v=1)$. The experimental $(v=1)/(v=0)$ signal ratio was calculated using the intensity of the relevant features in the experimental ion images. Reassuringly, the ratio of the population weighted theoretical partial cross sections were found to follow qualitatively the wavelength dependent behaviour observed experimentally. In particular, a vibrational temperature of 298 K was found to model the experimental data reasonably well, within the combined errors of the experiment, as shown in Fig. 4. It should be born in mind that the nozzle temperature can be elevated somewhat above ambient as a result of poor heat transfer in the vacuum, so the precise temperature of the Cl_2 gas immediately prior to expansion is not known.

Notwithstanding uncertainties in the measurement, the simulations suggest that there is little or no cooling of the vibrational degree of freedom in the molecular beam. By contrast, as shown in Subsection IV D, near limiting β param-

eters have been observed in the same experiments, consistent with efficient cooling of the rotational degree of freedom. In general, cooling of the rotational degrees of freedom is much more efficient than for vibrations in supersonic molecular beams.^{38,39} Aside from hydrogen, which has a very large rotational constant, the rotational energy of molecules in a molecular beam is equilibrated within tens of collisions and the energy removed from rotation converted to translational energy along the direction of flow of the beam. For vibrations of energy $>k_B T$, it may take an order of magnitude more collisions for the vibrational energy to be equilibrated, and the cooling of these in a molecular beam can therefore be very inefficient.

D. $\text{Cl}(^2P_{1/2})/\text{Cl}(^2P_{3/2})$ branching fraction and β parameter

Figure 5(a) displays the theoretical $\text{Cl}(^2P_{1/2})/\text{Cl}(^2P_{3/2})$ branching fraction for the $\text{Cl}_2(v=1)$ calculation. The branching fraction is defined, as previously,^{9–11}

$$\text{Cl}^*/\text{Cl} = \frac{\sigma_{\text{Cl}^*}}{\sigma_{\text{Cl}^*} + 2\sigma_{\text{Cl}}}, \quad (10)$$

where σ_{Cl^*} and σ_{Cl} represent the sum of the partial cross sections for the ground and excited state product channels, respectively. Also shown are the previously reported theoretical values for the photodissociation of $\text{Cl}_2(v=0)$.¹⁰ The excited state product channel becomes significant at much longer wavelengths, ~ 420 nm, relative to the dissociation from $\text{Cl}_2(v=0)$, for which the $\text{Cl}(^2P_{1/2})$ products start to increase in population near 370 nm. Furthermore, the slope of branching fraction, $\text{Cl}(^2P_{1/2})/\text{Cl}(^2P_{3/2})$, versus wavelength is much steeper for the $\text{Cl}_2(v=1)$ species, reflecting the gradients of the partial cross sections for the $C^1\Pi_{1u}$ and $B^3\Pi_{0^+u}$ states in the region 420–440 nm, and ultimately gives rise to relatively more excited state products in the long wavelength region. As with the $\text{Cl}_2(v=0)$ data, in general the experimental measurements appear to be in good agreement with the theoretically predicted branching fraction. The sharp spike in the calculated branching fraction near 340 nm can be understood in terms of the minima in the partial cross sections correlating with the ground state product channel, see Fig. 3(a).

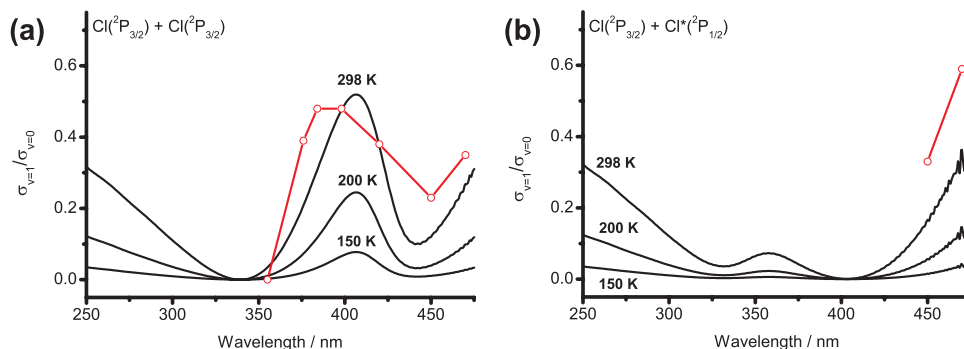


FIG. 4. The ratio of partial photodissociation yields (in black) from the $\text{Cl}_2(v=0)$ and $\text{Cl}_2(v=1)$ calculations, i.e., $\sigma_{v=1}/\sigma_{v=0}$ weighted by the initial state vibrational populations at the given temperature. The calculated data are compared with the experimental $(v=1)/(v=0)$ ratio (in red, with points) determined from the intensities of the $v=1$ and $v=0$ signals in the ion images. The experimental errors are typically around 10% for the $\text{Cl} + \text{Cl}$ channel, and somewhat larger for the $\text{Cl} + \text{Cl}^*$ channel. The calculations are based on vibrational temperatures of 150, 200, and 298 K. The data shown in (a) and (b) correspond to the ground ($\text{Cl} + \text{Cl}$) and excited ($\text{Cl} + \text{Cl}^*$) state product channels, respectively.

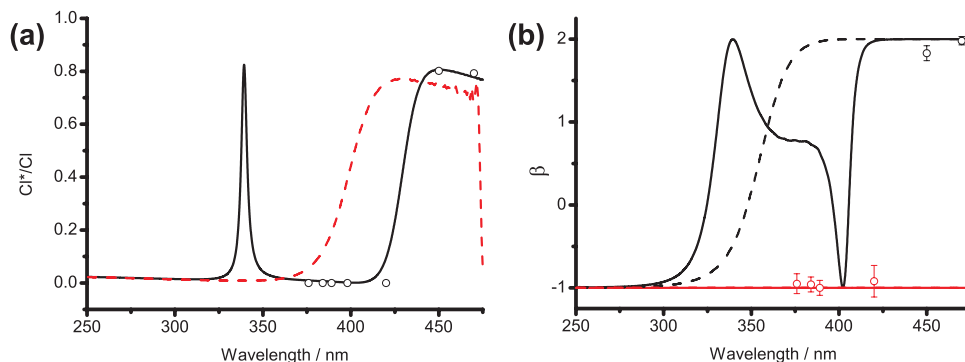


FIG. 5. (a) The branching fraction, Cl^*/Cl , as defined in the text, for $\text{Cl}_2(v=1)$ (—) and $\text{Cl}_2(v=0)$ (---) (shown in red). The experimental $v=1$ data are shown as black open circles. (b) Spatial anisotropy parameter, β , for $\text{Cl}_2(v=1)$ (—) and $\text{Cl}_2(v=0)$ (---). In this panel, the experimental data are represented by open circles, with red points and lines corresponding to the ground state product channel ($\text{Cl} + \text{Cl}$) and black points and lines to the excited product channel ($\text{Cl} + \text{Cl}^*$).

At 340 nm, the partial cross sections for both the $\text{C}^1\Pi_{1u}$ and $\text{A}^3\Pi_{1u}$ states are very small, and only the $\text{B}^3\Pi_{0+u}$ state contributes significantly to the dissociation. Since the $\text{B}^3\Pi_{0+u}$ state is associated with the excited state product channel, a sharp peak is observed in the $\text{Cl}(\text{P}_{1/2})/\text{Cl}(\text{P}_{3/2})$ branching fraction. Observation of this peak in the Cl^*/Cl branching fraction would provide a very stringent test of the quality of the potential energy curves employed in the dynamical calculations. However, its measurement is likely to require initial excitation of Cl_2 into ($v=1$), since otherwise the signal at around 340 nm is dominated by that from $\text{Cl}_2(v=0)$, and photodissociation from $\text{Cl}_2(v=1)$ is difficult to observe.

The spatial anisotropy parameter, β , for both dissociation channels is shown in Fig. 5(b). As with the dissociation of $\text{Cl}_2(v=0)$, the angular distribution of the ground state ($\text{Cl} + \text{Cl}$) product channel is seen to be wavelength independent and characterized by $\beta = -1$. Experimental measurements for this dissociation channel at all wavelengths are in good accord with the theory, and all are within error of the predicted limiting value. For the excited state ($\text{Cl} + \text{Cl}^*$) product channel, the β parameter is strongly wavelength dependent, reaching a limiting value for a parallel transition at long wavelengths, similar to the dissociation of $\text{Cl}_2(v=0)$. Near 400 nm the β parameter for this channel suddenly drops from a limiting +2 to -1. At this wavelength a minimum appears in the partial cross section for the $\text{B}^3\Pi_{0+u}$ state, Fig. 3(b), with the only non-zero contributions to the dissociation channel arising from the $(1)^3\Sigma_{1u}^+$ and $(1)^3\Delta_{1u}$ states. Population in both of these $\Omega = 1$ states, either by direct photon absorption, or indirectly following a transition to the $\text{C}^1\Pi_{1u}$ state, results in a β of -1 at this wavelength. Moving to shorter wavelengths, β increases rapidly towards positive values, reflecting the relative importance of the $\text{B}^3\Pi_{0+u}$, $(1)^3\Sigma_{1u}^+$, and $(1)^3\Delta_{1u}$ states, and again reaching a limiting value of +2 at 340 nm. At this wavelength, as mentioned above with regards to the spin-orbit branching fraction, a minimum appears in the partial cross section for the $\text{C}^1\Pi_{1u}$ state, and thus also for both the $(1)^3\Sigma_{1u}^+$ and $(1)^3\Delta_{1u}$ states, and only the parallel transition to the $\text{B}^3\Pi_{0+u}$ state makes a significant contribution to the dissociation. Beyond 340 nm, the β parameter declines sharply to -1 as the short wavelength wing of the $\text{B}^3\Pi_{0+u}$ state partial cross section decreases to zero.

Given the low $\text{Cl}(\text{P}_{1/2})/\text{Cl}(\text{P}_{3/2})$ branching fraction at wavelengths <420 nm, dissociation of $\text{Cl}_2(v=1)$ into the excited state product channel was only observed experimentally at two wavelengths, both in the long wavelength tail of the absorption. The experimental β parameter data at 470 nm are in good agreement with the theoretical value of +2, with the value determined for dissociation at 450 nm slightly smaller at 1.82, but in agreement with the results observed for $v=0$.¹⁰ The experimental β and polarization parameters, discussed in Subsection IV E, are summarized in Table IV.

As noted in Sec. IV B, branching fractions for the photodissociation of $\text{Cl}_2(v=0)$ and ($v=1$) have also been determined previously in the adiabatic calculations presented by Kokh *et al.*¹¹ One would not expect the branching fractions from the non-adiabatic calculations to differ significantly from the previous adiabatic results, and any slight differences that are observed primarily reflect the alternative approaches employed to the smoothing or fitting the potential curves.^{9–11} Given that the $\text{C}^1\Pi_{1u}$ and $\text{A}^3\Pi_{1u}$ both correlate with ground state $\text{Cl} + \text{Cl}$ photofragments, non-adiabatic transfer from the $\text{C}^1\Pi_{1u}$ to the $\text{A}^3\Pi_{1u}$ state will not affect the Cl^*/Cl branching fraction. Similarly, population of the $\text{Cl}^* + \text{Cl}$ channel at long wavelengths is dominated by absorption to, and adiabatic dissociation on, the $\text{B}^3\Pi_{0+u}$ state, and is thus unaffected by inclusion of non-adiabatic effects. Furthermore, while non-adiabatic transitions from the $\text{C}^1\Pi_{1u}$ to the $(1)^3\Sigma_{1u}^+$ and $(1)^3\Delta_{1u}$ are responsible for Cl^* production at short wavelengths, the yield of Cl^* is very small in this region in which these states participate (~ 320 nm), because photodissociation is dominated by excitation to, and adiabatic dissociation on the $\text{C}^1\Pi_{1u}$ state.

As noted previously,^{9,12–14} since more than one $\Omega = 1$ state correlates with the excited state channel, measurements of β alone are unable to resolve the precise mechanism for the formation of these products. Moreover, measurements of the translational anisotropy for the ground state product channel, for which $\beta = -1$ across the entire absorption band, are unable to shed light on which of the $\Omega = 1$ symmetry states are involved. Some of these issues are resolved in Sec. IV E, which considers the angular momentum polarization of the atomic photofragments.

TABLE IV. Spatial anisotropy and angular momentum polarization parameters for the $\text{Cl}(^2\text{P}_{3/2})$ fragments as returned from the fits to experimental Fourier moments. For wavelengths 376–420 nm, the data shown are for the ground state ($\text{Cl} + \text{Cl}$) product channel. For 450 nm and 470 nm, the data correspond to the excited state ($\text{Cl} + \text{Cl}^*$) product channel. Errors (1σ) in the last digit(s) are given in parentheses.

Parameter	Wavelength (nm)					
	376	384	389	420	450	470
β	−0.95(12)	−0.96(9)	−1.00(9)	−0.92(19)	1.83(9)	1.98(5)
s_2	−0.17(5)	−0.16(4)	−0.14(3)	−0.13(4)	−0.14(3)	−0.16(3)
α_2	−0.09(3)	−0.08(3)	−0.05(2)	−0.06(4)	0.13(3)	0.16(5)
γ_2	−0.24(10)	−0.15(7)	−0.01(2)	−0.13(5)	−0.03(3)	−0.10(9)
η_2	0.10(7)	−0.02(5)	0.05(5)	0.04(3)	0.00(2)	−0.01(3)
α_1	0.08(3)	0.16(4)	0.16(4)	0.09(4)	0.03(2)	...
γ_1	−0.07(4)	−0.03(4)	−0.09(5)	0.00(2)	−0.08(8)	...
γ_1'	0.05(7)	−0.02(4)	0.01(5)	0.00(5)
α_3	0.05(7)	−0.36(13)	−0.39(23)	0.00(1)	−0.05(14)	...
γ_3	0.31(16)	−0.15(5)	−0.38(26)	0.04(1)	−0.37(33)	...
γ_3'	0.16(39)	0.05(3)	0.51(33)	0.08(2)
η_3	−0.19(10)	0.36(9)	0.09(23)	0.02(1)

E. Angular momentum polarization

1. $\text{Cl}(^2\text{P}_{3/2})$ from the excited state ($\text{Cl} + \text{Cl}^*$) channel

At wavelengths longer than 420 nm the dissociation of $\text{Cl}_2(v=1)$ into the excited state ($\text{Cl} + \text{Cl}^*$) product channel can be viewed as an adiabatic process taking place on the $\text{B } ^3\Pi_{0+u}$ state potential. In this region, the calculated spatial anisotropy parameter is $\beta = +2$, and only non-zero incoherent polarization parameters are expected. The values of s_2 and α_2 , -0.16 and $+0.16$, respectively, are consistent with this picture, and zero contributions are expected to arise from coherent processes. As shown in Figs. 6(a) and 6(b), the experimental data in this region are in excellent agreement with these theoretical predictions. The only other previous experimental determination of the Cl atom polarization following the photodissociation of $\text{Cl}_2(v=1)$ was conducted at 470 nm by Zare and co-workers.⁸ They observed an alignment parameter $a_0^{(2)}(\parallel) = -0.8$, which corresponds to the limiting value for a pure parallel transition. It may be recalled that in this case $\alpha_2 = -s_2$ and that $a_0^{(2)}(\parallel) = 5(s_2 - 2\alpha_2)/(1 + \beta)$.⁴⁰ This result is therefore entirely consistent with the present experimental and theoretical results at this wavelength.

Moving to shorter wavelengths, the magnitudes of both s_2 and α_2 are calculated to decrease sharply, reaching a minimum near 400 nm, as shown in Fig. 6(a). Note that experimental measurements in this wavelength region become difficult, because of the very small branching fraction into the excited state product channel (see Subsection IV D). As mentioned previously with regards to the $\text{Cl}(^2\text{P}_{1/2})/\text{Cl}(^2\text{P}_{3/2})$ branching fraction and β parameter, a minimum appears in the partial cross section for the $\text{B } ^3\Pi_{0+u}$ state near this wavelength. In the region 340–400 nm, the calculated incoherent parameters follow the same trend as a function of wavelength as observed for the spatial anisotropy parameter, Fig. 5(b), reflecting the relative importance of the $\text{B } ^3\Pi_{0+u}$, $(1)^3\Sigma_{1u}^+$ and $(1)^3\Delta_{1u}$ states to the dissociation in this region. The coherent mixture of both dissociation via parallel and perpendicular transitions gives rise to non-zero values for the coherent alignment parameters. Specifically, interference between parallel and perpendicular pathways leads to non-zero values for the γ_2 parameter, while interference between the two components of a perpendicular transition lead to non-zero η_2 values. As seen from Fig. 6(b) both coherent parameters show oscillatory structure in this wavelength region, resulting from interferences between the different parallel

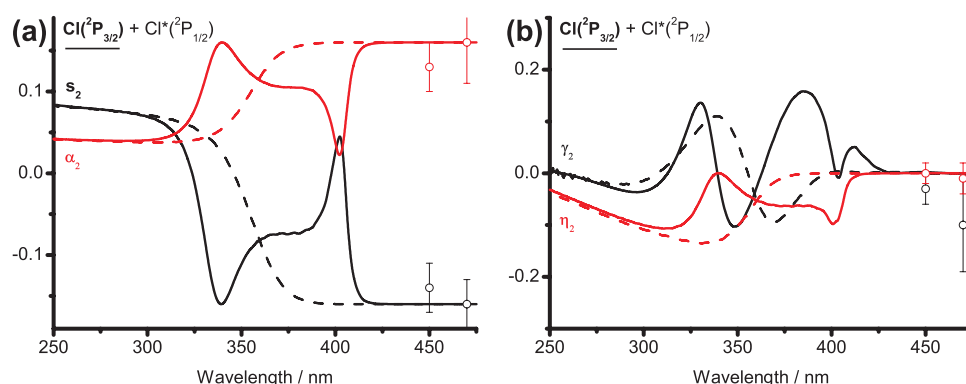


FIG. 6. Incoherent (a) and coherent (b) $K=2$ alignment parameters for $\text{Cl}_2(v=1)$ (—) and $\text{Cl}_2(v=0)$ (---) photodissociation into the excited state product channel ($\text{Cl} + \text{Cl}^*$). The experimental $v=1$ data returned from the fits to the $\text{Cl}(^2\text{P}_{3/2})$ Fourier moments are represented by open circles.

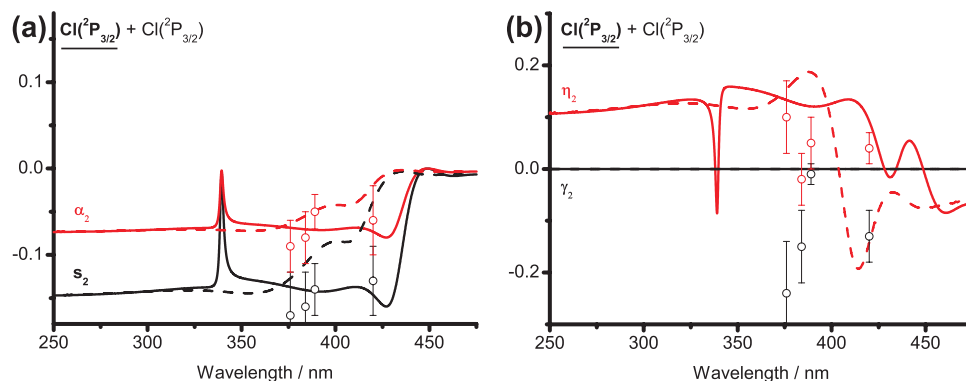


FIG. 7. Incoherent (a) and coherent (b) $K = 2$ alignment parameters for $\text{Cl}_2(v = 1)$ (—) and $\text{Cl}_2(v = 0)$ (---) photodissociation into the ground state product channel ($\text{Cl} + \text{Cl}$). The experimental $v = 1$ data returned from the fits to the $\text{Cl}({}^2P_{3/2})$ Fourier moments are represented by open circles.

and perpendicular pathways taken to the excited dissociation channel.

At 340 nm the minima in the $(1)^3\Sigma_{1u}^+$ and $(1)^3\Delta_{1u}$ state partial cross sections means the dissociation occurs predominantly adiabatically on the $\text{B } {}^3\Pi_{0+u}$ state potential, and so s_2 and α_2 reach limiting values. The coherent parameters γ_2 and η_2 are predicted to both go to zero at this wavelength, as shown in Fig. 6(b), illustrating the predominantly adiabatic nature of the process at this exact wavelength. Below 300 nm, contributions to the dissociation channel from the $\text{B } {}^3\Pi_{0+u}$ state are very small, and the coherent γ_2 parameter approaches zero. Here, only the perpendicular $(1)^3\Sigma_{1u}^+$ and $(1)^3\Delta_{1u}$ states are involved and so $s_2 = 2\alpha_2$, with non-zero values of η_2 also predicted.

2. $\text{Cl}({}^2P_{3/2})$ from the ground state ($\text{Cl} + \text{Cl}$) channel

The $K = 2$ alignment for the ground state product channel is shown in Fig. 7. As with the dissociation of $\text{Cl}_2(v = 0)$, at short wavelengths the dissociation may be viewed as a mostly adiabatic process taking place on the $\text{C } {}^1\Pi_{1u}$ state potential. Below 325 nm the incoherent parameter s_2 is close to the limiting value of -0.16 , with $s_2 = 2\alpha_2$, as expected following a perpendicular transition to the $\text{C } {}^1\Pi_{1u}$ state and an adiabatic dissociation. The sharp structure seen at 340 nm is a consequence of the minimum in the partial cross section for the $\text{C } {}^1\Pi_{1u}$ state. Interestingly, the incoherent parameters s_2 and α_2 appear roughly symmetrical for around 75 nm on either side of the minimum at 340 nm, reflecting the double peaked structure in the partial cross sections, as shown in Fig. 3. Around 425 nm, the incoherent alignment parameters decrease in magnitude. This reduction takes place at longer wavelengths than that seen for $\text{Cl}_2(v = 0)$. The decrease in magnitude of the incoherent parameters for $\text{Cl}_2(v = 0)$ was understood to reflect the increasing importance of the non-adiabatic pathway to the dissociation. Note that for $\text{Cl}_2(v = 1)$ the decrease of s_2 and α_2 to near-zero with increasing wavelength occurs much more rapidly than the gradual decrease seen for $\text{Cl}_2(v = 0)$. The experimental measurements of these parameters are in excellent agreement with the theoretical values.

Similar to the dissociation of $\text{Cl}_2(v = 0)$, within the current theoretical model no parallel $\Omega = 0$ state is involved in the dissociation into the ground state ($\text{Cl} + \text{Cl}$) product channel, and because of the absence of coherent excitation of parallel and perpendicular pathways, the coherent alignment parameter γ_2 is equal to zero. Nevertheless, small non-zero values of the γ_2 parameter are observed around 400 nm. The implications for appearance of the γ_2 parameter are that a parallel transition to an $\Omega = 0$ state is somehow involved in the dissociation. An $\Omega = 0$ state may be involved either through Coriolis ($\Delta\Omega = \pm 1$) electronic-rotational coupling of the $\text{C } {}^1\Pi_{1u}$ state with an $\Omega = 0$ state or more directly by optical excitation from the ground state to an $\Omega = 0$ state not included in the present theoretical model. Given the low parent molecule rotational temperature, the latter seems the most likely in the present case. We have shown in our previous work on $\text{Cl}_2(v = 0)$ that even relatively small contributions from direct excitation to an $\Omega = 0$ state could yield significant non-zero values of γ_2 , while at the same time not leading to significant deviations of β from its near-limiting value.⁹ The η_2 parameter, which arises from interference between the $\text{C } {}^1\Pi_{1u}$ and $\text{A } {}^3\Pi_{1u}$ state pathways, shows similar short wavelength behaviour to that following $\text{Cl}_2(v = 0)$ photodissociation. The change in sign of this parameter, however, occurs at longer wavelengths than observed for $\text{Cl}_2(v = 0)$ reflecting the differences in the importance of the $\text{C } {}^1\Pi_{1u}$ to $\text{A } {}^3\Pi_{1u}$ state non-adiabatic transition, as discussed above with respect to the incoherent alignment parameters. The experimental data seem to be in reasonable accord with theory, although in less good agreement than for the incoherent alignment parameters.

Both $K = 1$ and $K = 3$ incoherent orientation parameters have also been measured experimentally for photodissociation of $\text{Cl}_2(v = 1)$ into ground state ($\text{Cl} + \text{Cl}$) products, as shown in Fig. 8. The α_1 parameter is wavelength independent, since only the $\text{C } {}^1\Pi_{1u}$ and $\text{A } {}^3\Pi_{1u}$ states are involved in the dissociation, as discussed in Ref. 9 with regards to the orientation for dissociation of $\text{Cl}_2(v = 0)$. The α_3 parameter, however, like the incoherent alignment parameters, is roughly symmetrical about the minimum at 340 nm, reflecting the nodal structure seen in the partial photodissociation cross sections. At longer wavelengths, this parameter decreases in

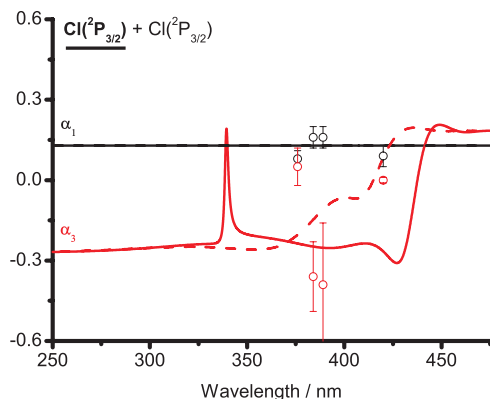


FIG. 8. Incoherent $K = 1$ and 3 orientation parameters for $\text{Cl}_2(v = 1)$ (—) and $\text{Cl}_2(v = 0)$ (---) dissociation into the ground state product channel ($\text{Cl} + \text{Cl}$). The experimental $v = 1$ data returned from the fits to $\text{Cl}({}^2\text{P}_{3/2})$ Fourier moments are represented by open circles.

magnitude as a result of the increasing importance of non-adiabatic effects.

V. CONCLUSIONS AND FUTURE WORK

The photodissociation of vibrationally excited $\text{Cl}_2(v = 1)$ has been investigated experimentally in detail over a range of wavelengths. Employing a combination of both experiment and theory it has been shown that negligible cooling of the vibrational degree of freedom of the parent molecule takes place in the molecular beam. Although the electronic states involved in the photodissociation of $\text{Cl}_2(v = 1)$ were found to be the same as for $\text{Cl}_2(v = 0)$, significant differences were found regarding the experimental observables. The differences were discussed in terms of the partial cross sections for photodissociation into the two product channels, ($\text{Cl} + \text{Cl}$) and ($\text{Cl} + \text{Cl}^*$). Good agreement was generally observed between the experimental measurements and the theoretical calculations, particularly for the branching fractions, translational anisotropy parameters, and incoherent alignment parameters. The coherent polarization parameters were somewhat less well reproduced by the theory, although they were still able to recover the qualitative behaviour observed experimentally as a function of wavelength.

Regarding future work on the photodissociation of vibrationally excited Cl_2 , it would be interesting to investigate the dynamics at shorter wavelengths than those probed here. In particular, it would be useful to study the region around 340 nm where a minimum appears in both partial cross sections of the states correlating with the $\text{Cl}({}^2\text{P}_{3/2}) + \text{Cl}({}^2\text{P}_{3/2})$ product channel. At this wavelength, a sharp peak in the $\text{Cl}({}^2\text{P}_{1/2})/\text{Cl}({}^2\text{P}_{3/2})$ branching fraction is expected as nearly all molecules dissociate to the excited state product channel. Measurements in this region would prove a stringent test of the current *ab initio* potentials. The study of the effect of chlorine isotope on the orientation moments would also be of interest, particularly if these measurements could be made on the Cl^* photofragments at wavelengths shorter than around 400 nm.^{9,41}

In the present study, the coherences between photofragments in different M_J levels have been investigated. By using femtosecond techniques, however, it may be possible to probe coherences between the $\text{Cl}({}^2\text{P}_J)$ spin-orbit states of the photofragments in future experimental studies. Further possibilities for new experiments on this system include the investigation of electronic polarization effects following the photodissociation of a coherently prepared sample of Cl_2 in ($v = 0$) and ($v = 1$). In addition, the current theoretical treatment of polarization effects in photodissociation deals with the case in which only one of the photofragments is detected. It may be possible, however, to use ion imaging techniques to probe the electronic polarization of the two fragments born in coincidence. In a system such as Cl_2 , in which all useful dynamical information can be derived through observation of only one fragment, this may not reveal new information. However, in general, the simultaneous detection of the atomic polarization of both photofragments could reveal fascinating new information on molecular photodissociation.

ACKNOWLEDGMENTS

The support of the Engineering and Physical Sciences Research Council (U.K.) (EPSRC(GB)) (to M.B. via Programme Grant No. EP/G00224X/1), the European Union (EU) (to M.B. via FP7 EU People ITN Project No. 238671) and the Deutsche Forschungsgemeinschaft (DFG) (to R.J.B. via Grant No. BU 450/21-2). A.B. thanks the Natural Sciences and Engineering Research Council of Canada (Discovery Grant) for financial support.

- ¹F. F. Crim, *J. Phys. Chem.* **100**, 12725 (1996).
- ²R. L. V. Wal, J. L. Scott, F. F. Crim, K. Weide, and R. Schinke, *J. Chem. Phys.* **94**, 3548 (1991).
- ³A. B. Alekseyev, H.-P. Liebermann, D. B. Kokh, and R. J. Buenker, *J. Chem. Phys.* **113**, 6174 (2000).
- ⁴J. P. Camden, H. A. Bechtel, D. J. A. Brown, A. E. Pomerantz, R. N. Zare, and R. J. Le Roy, *J. Phys. Chem. A* **108**, 7806 (2004).
- ⁵A. B. Alekseyev, D. B. Kokh, and R. J. Buenker, *J. Phys. Chem. A* **109**, 3094 (2005).
- ⁶A. B. Alekseyev, H.-P. Liebermann, R. J. Buenker, and S. N. Yurchenko, *J. Chem. Phys.* **126**, 234102 (2007).
- ⁷A. B. Alekseyev, H.-P. Liebermann, and R. J. Buenker, *J. Chem. Phys.* **126**, 234103 (2007).
- ⁸T. P. Rakitzis, S. A. Kandel, A. J. Alexander, Z. H. Kim, and R. N. Zare, *J. Chem. Phys.* **110**, 3351 (1999).
- ⁹E. K. Campbell, A. B. Alekseyev, G. G. Balint-Kurti, M. Brouard, A. Brown, R. J. Buenker, R. Cireasa, A. J. Gilchrist, A. J. Johnsen, D. B. Kokh, S. Lucas, G. A. D. Ritchie, T. R. Sharples, and B. Winter, *J. Chem. Phys.* **136**, 164311 (2012).
- ¹⁰A. J. Johnsen, A. B. Alekseyev, G. G. Balint-Kurti, M. Brouard, A. Brown, R. J. Buenker, E. K. Campbell, and D. B. Kokh, *J. Chem. Phys.* **136**, 164310 (2012).
- ¹¹D. B. Kokh, A. B. Alekseyev, and R. J. Buenker, *J. Chem. Phys.* **120**, 11549 (2004).
- ¹²A. S. Bracker, E. R. Wouters, A. G. Suits, and O. S. Vasyutinski, *J. Chem. Phys.* **110**, 6749 (1999).
- ¹³A. J. Alexander, Z. H. Kim, S. A. Kandel, R. N. Zare, T. P. Rakitzis, Y. Asano, and S. Yabushita, *J. Chem. Phys.* **113**, 9022 (2000).
- ¹⁴Y. Asano and S. Yabushita, *J. Phys. Chem. A* **105**, 9873 (2001).
- ¹⁵G. G. Balint-Kurti, A. J. Orr-Ewing, J. A. Beswick, A. Brown, and O. S. Vasyutinski, *J. Chem. Phys.* **116**, 10760 (2002).
- ¹⁶A. Brown, G. G. Balint-Kurti, and O. S. Vasyutinski, *J. Phys. Chem. A* **108**, 7790 (2004).
- ¹⁷A. G. Smolin, O. S. Vasyutinski, G. G. Balint-Kurti, and A. Brown, *J. Phys. Chem. A* **110**, 5371 (2006).

- ¹⁸P. M. Regan, D. Ascenzi, A. Brown, G. G. Balint-Kurti, and A. J. Orr-Ewing, *J. Chem. Phys.* **112**, 10259 (2000).
- ¹⁹A. Brown and G. G. Balint-Kurti, *J. Chem. Phys.* **113**, 1870 (2000).
- ²⁰C. C. Marston and G. G. Balint-Kurti, *J. Chem. Phys.* **91**, 3571 (1989).
- ²¹D. Kosloff and R. Kosloff, *J. Comput. Phys.* **52**, 35 (1983).
- ²²R. Kosloff, *J. Phys. Chem.* **92**, 2087 (1988).
- ²³A. Vibok and G. G. Balint-Kurti, *J. Phys. Chem.* **96**, 8712 (1992).
- ²⁴A. B. Alekseyev, H.-P. Liebermann, I. Boustani, G. Hirsch, and R. J. Buenker, *Chem. Phys.* **173**, 333 (1993).
- ²⁵A. B. Alekseyev, H.-P. Liebermann, and R. J. Buenker, "Spin-orbit multireference configuration interaction method and applications to systems containing heavy atoms," in *Recent Advances in Relativistic Molecular Theory*, edited by K. Hirao and M. Ishikawa (World Scientific, Singapore, 2003), p. 65.
- ²⁶G. G. Balint-Kurti, R. N. Dixon, and C. C. Marston, *Int. Rev. Phys. Chem.* **11**, 317 (1992).
- ²⁷E. J. Heller, *J. Chem. Phys.* **68**, 2066 (1978).
- ²⁸E. J. Heller, *J. Chem. Phys.* **68**, 3891 (1978).
- ²⁹E. J. Heller, *Acc. Chem. Res.* **14**, 368 (1981).
- ³⁰A. T. J. B. Eppink and D. H. Parker, *Rev. Sci. Instrum.* **68**, 3477 (1997).
- ³¹D. W. Chandler and P. L. Houston, *J. Chem. Phys.* **87**, 1 (1987).
- ³²M. Brouard, R. Cireasa, A. P. Clark, G. C. Groenenboom, G. Hancock, S. Horrocks, F. Quadrini, G. A. D. Ritchie, and C. Vallance, *J. Chem. Phys.* **125**, 133308 (2006).
- ³³M. Bass, M. Brouard, A. P. Clark, and C. Vallance, *J. Chem. Phys.* **117**, 8723 (2002).
- ³⁴M. Brouard, R. Cireasa, A. P. Clark, F. Quadrini, and C. Vallance, *Phys. Chem. Chem. Phys.* **8**, 5549 (2006).
- ³⁵M. Brouard, A. V. Green, F. Quadrini, and C. Vallance, *J. Chem. Phys.* **127**, 084304 (2007).
- ³⁶M. Brouard, F. Quadrini, and C. Vallance, *J. Chem. Phys.* **127**, 084305 (2007).
- ³⁷R. Schinke, *Photodissociation Dynamics: Spectroscopy and Fragmentation of Small Polyatomic Molecules* (Cambridge University Press, Cambridge, 1993).
- ³⁸*Atomic and Molecular Beam Methods: Volume 1*, edited by G. Scoles, D. Bassi, U. Buck, and D. C. Laine (Oxford University Press, 1988).
- ³⁹*Atomic and Molecular Beam Methods: Volume 2*, edited by G. Scoles, D. Bassi, U. Buck, and D. C. Laine (Oxford University Press, 1992).
- ⁴⁰A. G. Suits and O. S. Vasyutinskii, *Chem. Rev.* **108**, 3706 (2008).
- ⁴¹Z. H. Kim, A. J. Alexander, S. A. Kandel, T. P. Rakitzis, and R. N. Zare, *Faraday Discuss.* **113**, 27 (1999).